LETTER

Experimental investigation of the tilt angle of turbulent structures in the core of fusion plasmas

IOP Publishing | International Atomic Energy Agency Nuclear Fusion

Nucl. Fusion **59** (2019) 074002 (6pp) https://doi.org/10.1088/1741-4326/ab227e

Letter

Experimental investigation of the tilt angle of turbulent structures in the core of fusion plasmas

J.R. Pinzón[1,2], T. Happel[1], P. Hennequin[3], C. Angioni[1], T. Estrada[4], A. Lebschy[1], U. Stroth[1,2] and the ASDEX Upgrade Team[1]

[1] Max-Planck-Institut für Plasmaphysik, Garching, Germany
[2] Physik-Department E28, Technishe Universität München, Garching, Germany
[3] Laboratoire de Physique de Plasmas, Ecole Polytechnique, Palaiseau, France
[4] Laboratorio Nacional de Fusión, CIEMAT, Madrid, Spain

E-mail: javier.pinzon@ipp.mpg.de

Received 24 January 2019, revised 1 May 2019
Accepted for publication 17 May 2019
Published 5 June 2019

Abstract

The tilt angle of turbulent structures stands for the anisotropy of turbulence which is essential for understanding the dynamics of magnetized plasmas. It is a quantity predicted by theory and simulations, that provides information on the interplay between turbulence, micro-instabilities and plasma flows. A new method for measuring the tilt angle of turbulent structures in the core region of fusion plasmas using Doppler reflectometry is presented. First measurements of this type on the ASDEX Upgrade tokamak have shown a significant difference of tilt angle for different plasma conditions. The dominance of sheared $E \times B$ flows in determining the structure tilt is experimentally demonstrated for different turbulence regimes.

Keywords: plasma turbulence, sheared flow, microinstabilities, plasma diagnostics

(Some figures may appear in colour only in the online journal)

The dynamics of physical systems is frequently determined by turbulence. The macroscopic behaviour of fluids and plasmas can be closely related to the microscopic structures of turbulent fluctuations in density, temperature, and for plasmas, electric potential. In most plasmas, transport of particles, momentum and energy is governed by turbulence. Examples are found in astrophysics where turbulence is fundamental in the explosion mechanism of core-collapse supernovae [1], and also in magnetic fusion research where turbulence determines to a large extent the energy confinement time of the plasma [2].

In a magnetized plasma, turbulence can be considered as two-dimensional due to the high mobility of electrons and ions along the magnetic field. Therefore, in a simple description, *turbulent structures* can be described by an elliptical shape with characteristic size, elongation and tilt angle. This work addresses in particular the *tilt angle of turbulent structures* in the core of a fusion plasma. This quantity specifies the anisotropy of turbulence which is essential for the interaction with plasmas flows and instabilities [3].

Turbulence and $E \times B$ flows constitute a strongly coupled system [4]. A sheared $E \times B$ flow can tilt and stretch turbulent structures. If the $E \times B$ shear is strong enough, the structures are decorrelated leading to a reduction of the turbulence level [5]. At the same time, turbulence itself can generate $E \times B$ flows through the Reynolds stress mechanism, which requires a systematic variation of the structure tilt. This is the mechanism behind zonal flow generation [6], and residual stress contributions to transport of toroidal momentum [7].

Instabilities driving turbulence are characterized by a global *mode structure* whose symmetry is broken by the radial

variation of plasma parameters [8]. The radial direction is defined across the magnetic surfaces. A radial variation of the phase velocity of the unstable modes induces a systematic tilt of the structures as shown by analytical results from the linear ballooning theory [9] and simulations [8–10]. Moreover, different mode structures have been observed in gyrokinetic simulations of ion-temperature-gradient (ITG) and trapped-electron (TEM) modes [8]. They are the dominant micro-instabilities in the core of fusion plasmas at the ion scale i.e. with perpendicular wavenumbers $k_\perp$ in the range $k_\perp \rho_i \approx 0.2$–$1$ ($\rho_i = \sqrt{m_i T_i}/(eB)$ is the ion Larmor radius). The perpendicular direction is defined tangential to magnetic surfaces and perpendicular to the magnetic field.

Despite the importance of the tilt angle, its direct measurement in fusion plasmas remains challenging. Measurements have been provided using gas puff imaging [11, 12], Langmuir probes [13, 14], and beam emission spectroscopy [15, 16]. This letter presents a new method to measure the tilt angle of turbulent structures using Doppler reflectometry, which is a standard diagnostic technique based on the scattering of microwaves at electron density fluctuations [17]. It has the advantage of being non-invasive and applicable in the core of fusion plasmas where the best suited modelling tools, e.g. gyrokinetic simulations [18], are available. The new method is applied on discharges of the ASDEX Upgrade (AUG) tokamak for two parameter sets, and tilt angle measurements in the core region are reported for the first time. From the comparison of experimental measurements with simple models, the impact of mode structure and $E \times B$ shear on the tilt angle is assessed.

A low confinement plasma in lower single null magnetic configuration has been investigated. The plasma current is 0.8 MA and the toroidal magnetic field on-axis is 2.5 T. A neutral beam injection heating (NBI) power of 0.8 MW is applied during the complete plasma discharge. After an initial phase with only NBI external heating, 1.5 MW electron cyclotron resonance heating (ECRH) power is added. In the following, the two phases are labelled as 'NBI phase' and 'ECRH phase', respectively. The different heating systems are used to vary the electron to ion heat flux ratio and are intended to induce different turbulence regimes. In addition, short NBI blips are applied for obtaining charge exchange recombination spectroscopy (CXRS) measurements [19].

Figure 1 shows radial profiles of the main plasma parameters. The radial coordinate $\rho_{\rm pol}$ is the normalized poloidal flux radius. The plasma density in (*a*) is obtained from Thomson scattering [20] and lithium beam diagnostics [21]. The electron temperature profiles in (*b*) are obtained from Thomson scattering and electron cyclotron emission measurements [22]. The additional electron heating in the ECRH phase results in a higher electron temperature. The ion temperature in (*c*) obtained from CXRS measurements is rather similar for both phases. Nevertheless, the electron–ion collisional heat transfer increases slightly the ion temperature in the ECRH phase. The $E \times B$ drift velocity ($u_{E\times B}$) computed from CXRS measurements [19] is shown in figure 1(*d*) with solid lines. In the ECRH phase the velocity is approximately constant at about 8 km s^{-1}, whereas the NBI phase shows a strong shear

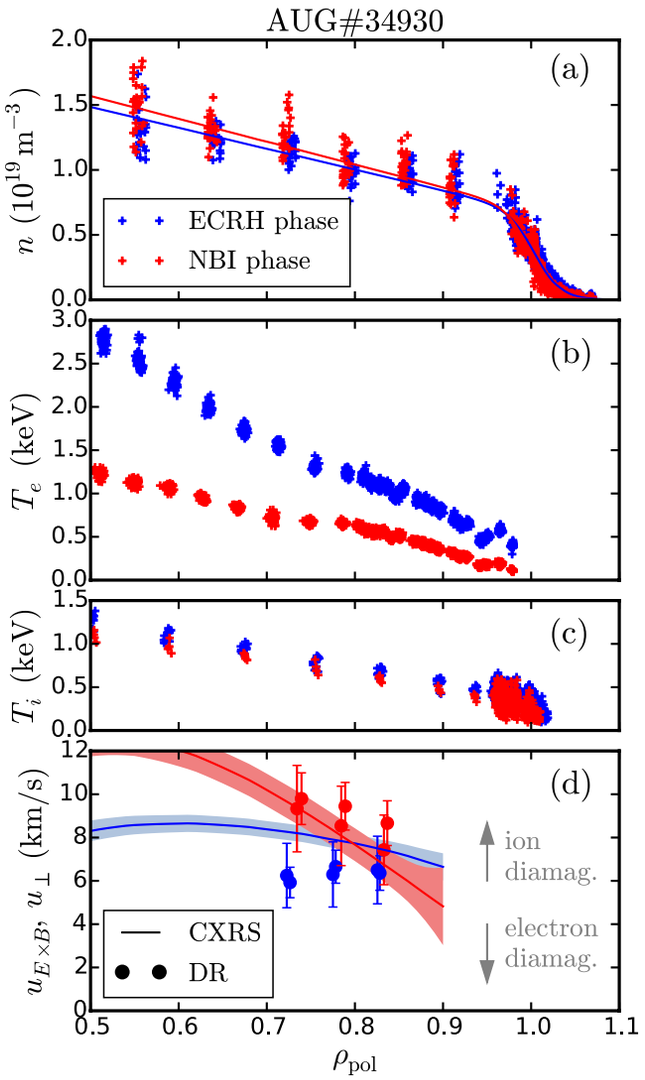

Figure 1. Radial profiles for ECRH and NBI phases of (*a*) plasma density, (*b*) electron temperature, (*c*) ion temperature and (*d*) plasma velocity. The $E \times B$ velocity is obtained from CXRS measurements (solid line) and the turbulence velocity $u_\perp$ from Doppler reflectometry measurements (circles).

as the velocity increases from about 5 km s^{-1} at $\rho_{\rm pol} = 0.9$ to 10 km s^{-1} at $\rho_{\rm pol} = 0.7$.

The experimental technique used in this letter for investigating turbulence is Doppler reflectometry [17]. A microwave beam is obliquely sent into the plasma from an antenna located outside. The beam propagates in the plasma and is reflected at the cutoff layer, where the refractive index is minimum and backscattering at density fluctuations with $k_\perp$ fulfilling the Bragg condition is strong. The backscattered wave propagates back to the antenna where it is detected. The frequency of the backscattered wave is Doppler shifted due to the perpendicular propagation velocity of the turbulent structures $u_\perp = u_{E\times B} + v_{\rm ph}$. It corresponds to the $E \times B$ flow and an intrinsic phase velocity $v_{\rm ph}$ in the plasma frame, which is characteristic of the type of turbulence. The frequency Doppler shift $f_{\rm D}$ provides a measurement of $u_\perp = 2\pi f_{\rm D}/k_\perp$.

Radial correlation Doppler reflectometry [23, 24] uses two beams probing simultaneously at radially displaced positions. The probing frequency of one beam (referred to as *reference*

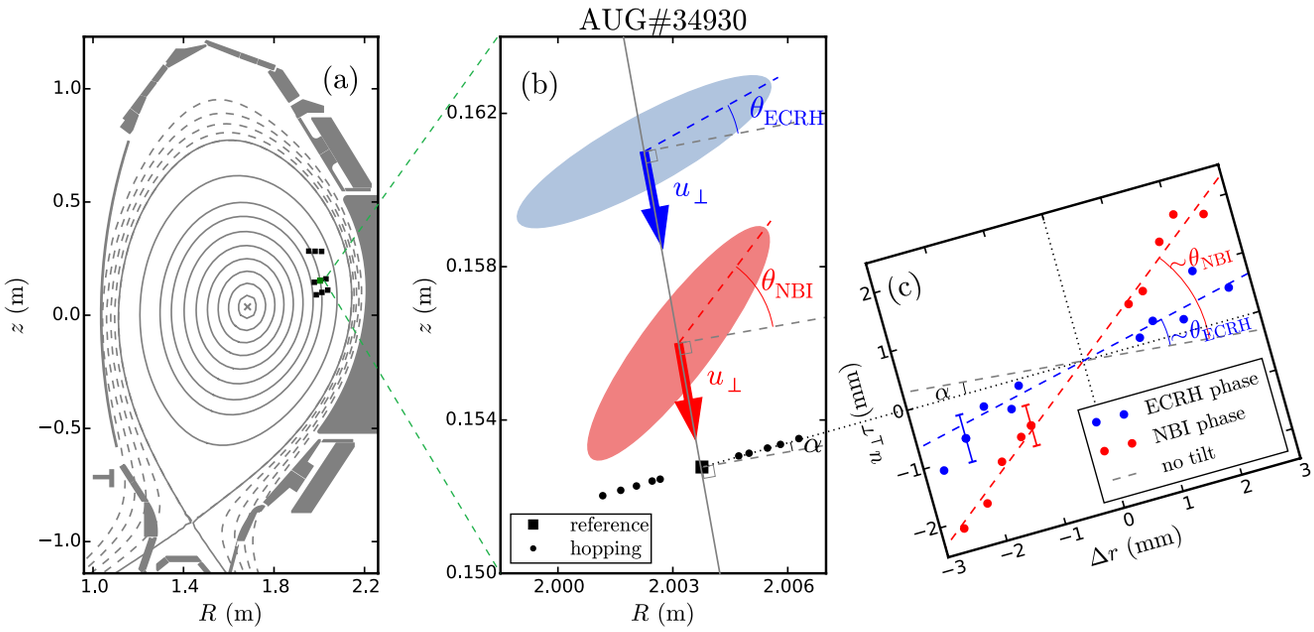

Figure 2. (*a*) Doppler reflectometry measurement positions on the AUG cross-section. (*b*) Enlargement showing the reference and hopping channel measurement positions in detail. Turbulent structures are schematically depicted, along with their tilt angle and propagation direction. (*c*) Time delay τ multiplied by $u_\perp$ as a function of the radial separation Δr. The grey dashed line indicates $u_\perp\tau$ for radially aligned structures, hence the angle formed by the measurement and this line gives approximately the tilt angle θ.

channel) is fixed whereas the frequency of the other one (*hopping channel*) is scanned. In the standard technique, the correlation level of the reflectometer signals and its dependence on the radial separation Δr are used for estimating the turbulent radial correlation length [23, 24]. In this letter, the time delay τ obtained from the correlation of the two reflectometer signals is used for measuring the tilt angle of turbulent structures.

Doppler reflectometry measurements have been performed with two V-band channels [25] coupled in X-mode polarization to the antenna system installed in AUG [26]. For the reference channel, probing frequencies of 69.0, 70.5 and 72.0 GHz (during 50 ms each) are used for three angles of incidence of the probing beam. The scattering position and the probed perpendicular wavenumber $k_\perp$ are obtained with the ray tracing code TORBEAM [27] and using fits to the density profiles (solid lines in figure 1(*a*)). The scattering positions are depicted with black squares on the AUG cross-section in figure 2(*a*). Closed and open magnetic surfaces are depicted with solid and dashed grey lines, respectively. Measurements are in the radial range $\rho_{\mathrm{pol}} = 0.70$–$0.84$ and at perpendicular wavenumbers $k_\perp$ within 3–8 cm^{-1}.

Results of the turbulence propagation velocity are shown with circles in figure 1(*d*). Although Doppler reflectometry measurements show a similar behaviour as CXRS data, there are systematic differences that suggest finite phase velocities v_{ph} with respect to $u_{E\times B}$. In the NBI phase, a positive v_{ph} in the ion diamagnetic direction indicates ion-driven turbulence, i.e. ITG. Contrarily in the ECRH phase, a negative v_{ph} in the electron diamagnetic direction indicates electron-driven turbulence, i.e. TEM. The dispersion of data may be a signature of a small variation of v_{ph} with $k_\perp$.

For the correlation measurements, the hopping channel probes ten frequencies (5 ms each) in a 0.15 GHz range around the reference channel frequency. In the following, the method to measure the tilt angle is presented for the case zoomed in figure 2(*b*). The measurement position of the reference and hopping channels are depicted with a square and circles, respectively. Note that due to the oblique incidence of the probing beam, the measurement positions are not aligned along the radial direction (dashed grey line), but form an angle α with respect to it. The time delays τ have been obtained from the time lag at the maximum of the cross-correlation function of reference and hopping channel signals. τ values have been multiplied by $u_\perp$ and plotted as function of the radial separation in figure 2(*c*). A linear dependence of $u_\perp\tau$ on Δr is observed. The dashed lines are linear fits to the data.

The measured time delays indicate that turbulent structures are tilted as depicted schematically in figure 2(*b*). As the structures propagate downwards, they are 'seen' first by the hopping channel for $\Delta r < 0$ and later by the reference one, obtaining a negative time delay. Complementary, for $\Delta r > 0$ the time delay is positive. The larger slope obtained in the NBI phase implies a stronger structure tilt than in the ECRH phase. In contrast, if structures are aligned with the measurement positions, a zero time delay is obtained as structures are simultaneously seen by reference and hopping channels. Figure 2(*c*) has been rotated accordingly.

Moreover, if structures are radially aligned, the grey dashed line is to be obtained in figure 2(*c*) because of the misalignment of the measurement positions by an angle α. Consequently, the tilt angle of the turbulent structures θ, defined with respect to the radial direction, can be approximated by the angle formed by the measurements and the grey dashed line as indicated in figure 2(*c*). This representation is intuitive and shows the principle of the measurement method. A more careful analysis of the geometry allows accurate calculation of the tilt angle from

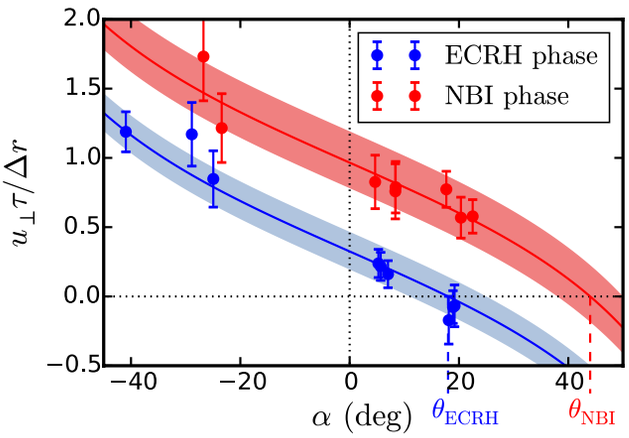

Figure 3. $u_\perp\tau/\Delta r$ values obtained from all reference positions as a function of the angle α. The solid lines depict the fit with equation (1) from which the average tilt angle is obtained.

$$\frac{u_\perp\tau}{\Delta r} = \tan\theta - \tan\alpha. \tag{1}$$

Note that $u_\perp\tau/\Delta r$ corresponds to the slope of the linear fits in figure 2(*c*).

The values of $u_\perp\tau/\Delta r$ obtained from all reference positions are shown as a function of the angle α in figure 3. For each phase, data are satisfactorily fitted with equation (1) and with a constant tilt angle (solid line). The tilt angles obtained from the fit are

$$\theta_{\rm ECRH} = (18 \pm 7)^\circ, \qquad \theta_{\rm NBI} = (44 \pm 6)^\circ. \tag{2}$$

Schematic structures with the corresponding tilt have been depicted in figure 2(*b*).

The significant difference between the tilt angle obtained for both phases proves that the method is applicable and that it provides results sensitive to plasma parameters. Further details on the method, its applicability to general experimental conditions, diagnostic effects related to the structure life time and finite scattering volume, will be presented in a future publication [28]. In the rest of this letter, the experimental measurements are compared with results from linear ballooning theory [10] in order to obtain a first estimate of the physical mechanisms which could potentially explain the observed differences in tilt angle. In this framework, the tilt angle is estimated by [10]

$$\theta \approx -\mathrm{sign}[\hat{s}(\partial_r v_{\rm ph} + \partial_r u_{E\times B})] \left| \frac{\partial_r v_{\rm ph} + \partial_r u_{E\times B}}{2\gamma\hat{s}} \right|^{1/3}, \tag{3}$$

where ∂_r denotes the radial derivative, γ the growth rate of the instability and $\hat{s}$ the magnetic shear. The effect of the instability mode structure is included through the shear of the mode velocity $\partial_r v_{\rm ph}$, and the effect of the $E \times B$ shear through $\partial_r u_{E\times B}$. The addition of both terms in the numerator indicates the competition of both physical mechanisms in the determination of the tilt angle.

In order to obtain the linear growth rate and phase velocities, the two plasma phases have been investigated with linear local gyrokinetic simulations using the code GKW [29].

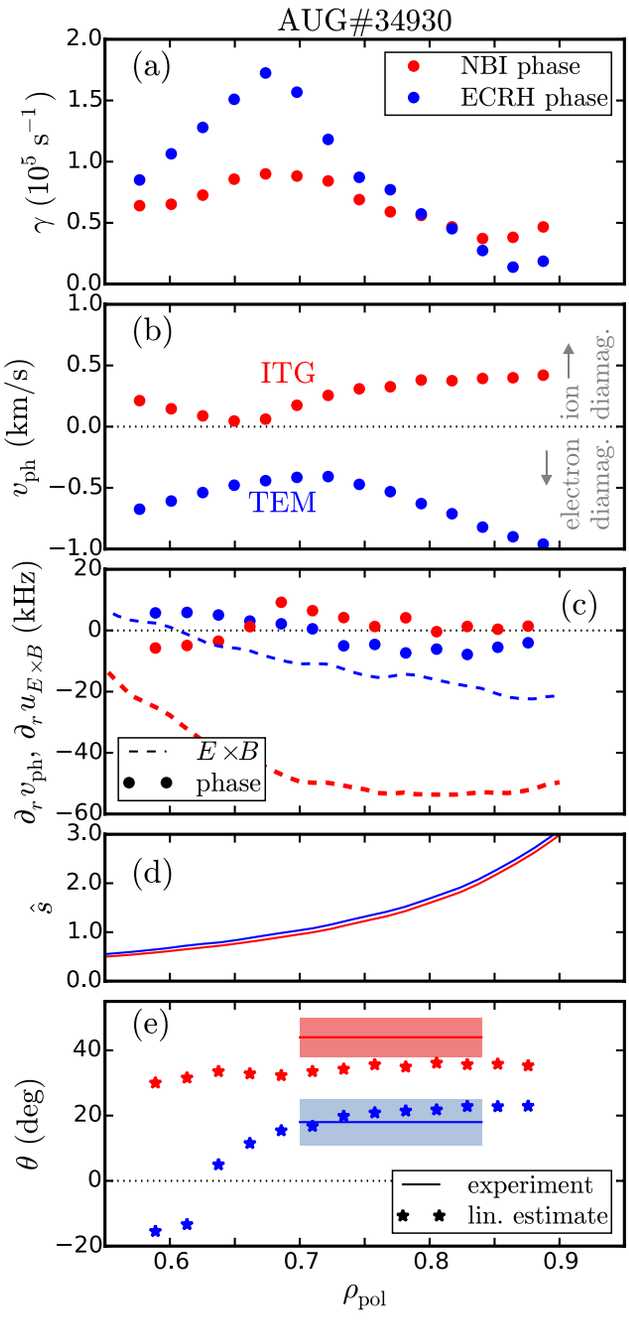

Figure 4. (*a*) Linear growth rate and (*b*) phase velocity obtained with GKW simulations. (*c*) $E \times B$ (dashed lines) and phase velocity (circles) shear. (*d*) Magnetic shear $\hat{s}$. (*e*) Tilt angle estimated with equation (3) (stars) and experimental measurements (solid line).

The experimental density and temperature profiles have been used as an input for the code. A linear stability analysis has been performed in the radial range of interest for the perpendicular wavenumber $k_\perp \approx 3.5$ cm^{-1} consistent with the experimental measurements and corresponding to the ion scale ($k_\perp\rho_i \approx 0.7$). The growth rates and phase velocities are presented in figures 4(*a*) and (*b*). The phase velocity points in the ion and electron diamagnetic directions for the NBI and ECRH phases, respectively. This confirms ITG and TEM dominated turbulence regimes, in agreement with the experimental indication of phase velocity in figure 1(*d*).

The velocity shear in figure 4(*c*) is obtained from GKW data ($\partial_r v_{\mathrm{ph}}$) and from CXRS measurements ($\partial_r u_{E\times B}$). The $E \times B$ shear is larger than the phase velocity shear in both cases, indicating that $E \times B$ shear is the dominant effect. In the NBI phase, a factor of 10 suggests that the tilt angle is determined by $E \times B$ shear only. In the ECRH phase, although the $E \times B$ shear dominates, the mode structure could still contribute weakly to the tilt angle.

The magnetic shear $\hat{s}$ plays also a role in determining the tilt angle as evidenced by equation (3). Magnetic shear profiles obtained from equilibrium reconstruction are shown in figure 4(*d*) for both phases. Since there is no significant difference, magnetic shear cannot account for the tilt angle change between both phases.

For the estimation of the tilt angle from equation (3), the maximum γ value in the radial scan corresponding to the most unstable mode has been taken for each phase. The results are shown in figure 4(*e*) (stars), together with the experimental measurements (see equation (2)). The linear estimate recovers qualitatively the stronger tilt for the NBI phase, moreover the values for the ECRH phase are within the experimental errorbars. Since equation (3) gives just an estimate for the linear case, an exact quantitative agreement is not expected. Nevertheless, the similarity of the magnitudes indicate that for the plasmas under investigation, the tilt angle is predominantly induced by the $E \times B$ shear.

For future studies, a better assessment of the mode structures can be achieved with global simulations [8–10]. Moreover the competition of both effects, mode structure and $E \times B$ shear, as well as non-linear interactions can be self-consistently treated with more advanced tools as non-linear global gyrokinetic simulations. It is possible that for scenarios with low $E \times B$ shear, the tilt angle measurement might provide a signature of the dominant turbulence regime.

In this letter, a novel measurement method of the tilt angle of turbulent structures has been proposed, and measurements in the core of the AUG tokamak have been presented for the first time. The comparison of the experimental measurements with simple models has demonstrated the dominant effect of sheared $E \times B$ flows on the structure tilt for ITG and TEM dominated turbulence. In the future, the systematic application of this technique can provide radially and temporally resolved measurements, with a few mm resolution and in the kHz range. This will enable a wealth of turbulence studies, for example of the local Reynolds stress and zonal flows, both fundamental elements for understanding the interactions of turbulence in plasmas.

Acknowledgments

This work has been carried out within the framework of the EUROfusion Consortium and has received funding from the Euratom research and training program 2014–2018 and 2019–2020 under Grant Agreement No. 633053. The views and opinions expressed herein do not necessarily reflect those of the European Commision.

ORCID iDs

J.R. Pinzón https://orcid.org/0000-0003-0621-5697
T. Happel https://orcid.org/0000-0003-4364-9363

References

[1] Radice D., Abdikamalov E., Ott C.D., Mösta P., Couch S.M. and Roberts L.F. 2018 Turbulence in core-collapse supernovae *J. Phys. G: Nucl. Part. Phys.* **45** 053003
[2] Doyle E.J. *et al* 2007 Chapter 2: Plasma confinement and transport *Nucl. Fusion* **47** S18
[3] Terry P.W. 2000 Suppression of turbulence and transport by sheared flow *Rev. Mod. Phys.* **72** 109–65
[4] Stroth U., Manz P. and Ramisch M. 2011 On the interaction of turbulence and flows in toroidal plasmas *Plasma Phys. Control. Fusion* **53** 024006
[5] Biglari H., Diamond P.H. and Terry P.W. 1990 Influence of sheared poloidal rotation on edge turbulence *Phys. Fluids* B **2** 1–4
[6] Diamond P.H., Itoh S.-I., Itoh K. and Hahm T.S. 2005 Zonal flows in plasma—a review *Plasma Phys. Control. Fusion* **47** R35
[7] Angioni C. *et al* 2011 Intrinsic toroidal rotation, density peaking, and turbulence regimes in the core of tokamak plasmas *Phys. Rev. Lett.* **107** 215003
[8] Camenen Y., Idomura Y., Jolliet S. and Peeters A.G. 2011 Consequences of profile shearing on toroidal momentum transport *Nucl. Fusion* **51** 073039
[9] Kim J.Y., Kishimoto Y., Wakatani M. and Tajima T. 1996 Poloidal shear flow effect on toroidal ion temperature gradient mode: A theory and simulation *Phys. Plasmas* **3** 3689–95
[10] Kishimoto Y., Kim J.-Y., Horton W., Tajima T., LeBrun M.J. and Shirai H. 1999 Toroidal mode structure in weak and reversed magnetic shear plasmas and its role in the internal transport barrier *Plasma Phys. Control. Fusion* **41** A663
[11] Shesterikov I., Xu Y., Tynan G.R., Diamond P.H., Jachmich S., Dumortier P., Vergote M., Van Schoor M., Van Oost G. and Team TEXTO R 2013 Experimental evidence for the intimate interaction among sheared flows, eddy structures, Reynolds stress, and zonal flows across a transition to improved confinement *Phys. Rev. Lett.* **111** 055006
[12] Zweben S.J., Stotler D.P., Scotti F. and Myra J.R. 2017 Two-dimensional turbulence cross-correlation functions in the edge of NSTX *Phys. Plasmas* **24** 102509
[13] Carter T.A. and Maggs J.E. 2009 Modifications of turbulence and turbulent transport associated with a bias-induced confinement transition in the Large Plasma Device *Phys. Plasmas* **16** 012304
[14] Guszejnov D., Bencze A., Zoletnik S. and Krämer-Flecken A. 2013 Determination of structure tilting in magnetized plasmas time delay estimation in two dimensions *Phys. Plasmas* **20** 062303
[15] Shafer M.W., Fonck R.J., McKee G.R., Holland C., White A.E. and Schlossberg D.J. 2012 2D properties of core turbulence on DIII-D and comparison to gyrokinetic simulations *Phys. Plasmas* **19** 032504
[16] Fox M.F.J., van Wyk F., Field A.R., Ghim Y.C., Parra F.I. and Schekochihin A.A. 2017 Symmetry breaking in MAST plasma turbulence due to toroidal flow shear *Plasma Phys. Control. Fusion* **59** 034002
[17] Hirsch M., Holzhauer E., Baldzuhn J., Kurzan B. and Scott B. 2001 Doppler reflectometry for the investigation of propagating density perturbations *Plasma Phys. Control. Fusion* **43** 1641

[18] Garbet X., Idomura Y., Villard L. and Watanabe T.H. 2010 Gyrokinetic simulations of turbulent transport *Nucl. Fusion* **50** 043002
[19] Lebschy A. *et al* 2018 Measurement of the complete core plasma flow across the LOC-SOC transition at ASDEX Upgrade *Nucl. Fusion* **58** 026013
[20] Murmann H., Götsch S., Röhr H., Salzmann H. and Steuer K.H. 1992 The Thomson scattering systems of the ASDEX Upgrade tokamak *Rev. Sci. Instrum.* **63** 4941–3
[21] Fischer R., Wolfrum E., Schweinzer J. and the ASDEX Upgrade Team 2008 Probabilistic lithium beam data analysis *Plasma Phys. Control. Fusion* **50** 085009
[22] Rathgeber S.K., Barrera L., Eich T., Fischer R., Nold B., Suttrop W., Willensdorfer M., Wolfrum E. and the ASDEX Upgrade Team 2013 Estimation of edge electron temperature profiles via forward modelling of the electron cyclotron radiation transport at ASDEX Upgrade *Plasma Phys. Control. Fusion* **55** 025004
[23] Schirmer J., Conway G.D., Holzhauer E., Suttrop W., Zohm H. and the ASDEX Upgrade Team 2007 Radial correlation length measurements on ASDEX Upgrade using correlation Doppler reflectometry *Plasma Phys. Control. Fusion* **49** 1019
[24] Fernández-Marina F., Estrada T. and Blanco E. 2014 Turbulence radial correlation length measurements using Doppler reflectometry in TJ-II *Nucl. Fusion* **54** 072001
[25] Sabot R., Hennequin P. and Colas L. 2009 Fluctuation measurements and their link with transport on Tore Supra *Fusion Sci. Technol.* **56** 1253–72
[26] Happel T. *et al* 2015 Core turbulence behavior moving from ion-temperature-gradient regime towards trapped-electron-mode regime in the ASDEX Upgrade tokamak and comparison with gyrokinetic simulation *Phys. Plasmas* **22** 032503
[27] Poli E. *et al* 2018 Torbeam 2.0, a paraxial beam tracing code for electron-cyclotron beams in fusion plasmas for extended physics applications *Comput. Phys. Commun.* **225** 36–46
[28] Pinzón J.R., Estrada T., Happel T., Hennequin P., Blanco E., Stroth U., the ASDEX Upgrade Team and the TJ-II Team 2019 Measurement of the tilt angle of turbulent structures in magnetically confined plasmas using Doppler reflectometry *Plasma Phys. Control. Fusion* submitted
[29] Peeters A.G., Camenen Y., Casson F.J., Hornsby W.A., Snodin A.P., Strintzi D. and Szepesi G. 2009 The nonlinear gyro-kinetic flux tube code GKW *Comput. Phys. Commun.* **180** 2650–72